

PARAMETRIC STUDIES OF THERMOGRAPHIC DETECTION OF DISBONDS IN
LAMINATED STRUCTURES USING COMPUTATIONAL SIMULATIONS

P. A. Howell^{*}, William P. Winfree, B. Scott
Crews^{*}, and Elliott Cramer
MS 231
NASA, Langley Research Center
Hampton, VA 23665

INTRODUCTION

A quantitative assessment of a structure's material characteristics contributes to the safety, reliability, and useful lifetime of a structure. Thermographic nondestructive evaluation has advantages over other methods in that it is a noncontacting, quantitative measurement of the material integrity which can inspect large areas in a short period of time. A disbond between layers of a laminated structure will prevent heat from penetrating from the surface layer to the subsurface layers and will result in an increase in temperature over the disbond. The limits of this technique for detection of disbonds in solid rocket motors was investigated by computational simulation of the thermographic technique. This has an advantage over an experimental investigation, since many sample configurations and flaw sizes can be investigated at a fraction of the cost and time required for sample fabrication, data acquisition and analysis. This paper presents a series of simulations varying parameters that affect the thermal contrast such as heating time, disbond size, and thickness of the surface layer. Experimental results are presented for comparison.

FINITE ELEMENT THEORY

A finite element heat transfer algorithm developed at Lawrence Livermore National Laboratory was used to model the laminated structure [1]. A variety of initial conditions and boundary conditions can be specified, including flux or convection boundaries. Materials are specified by their material properties including density, specific heat and thermal conductivity. Disbonds at material interfaces are modeled by the use of slidelines. A slideline specifies the contact resistance between two nodes in the model. The magnitude of the contact resistance at the slide line is specified to model the flaw. To generate the grid necessary for the finite element solution, an algorithm was developed using a hyperbolic sine transformation equation [2]. The transformation

^{*}Analytical Services & Materials, Inc.

equation is used to refine the grid about the material interface and the disbond, where the temperature gradients will be largest, and smoothly increase the spacing as the grid moves away from this boundary.

RESULTS

Variations With Heating Duration

The first set of simulations investigated the effects of varying heating time on the temperature contrast. A two dimensional simulation of a three layered structure was performed, with a defect at the center of one of the interfaces. This model is equivalent to a structure with a long thin disbond. The thermal properties of the layers were chosen to correspond to the thermal properties of the three major layers of the shuttle solid rocket motor (steel, NBR insulation and fuel) shown in Table I. For the heating phase of the simulation, the front surface boundary condition was chosen to simulate application of water at 30°C above ambient ($T_{\infty}+30^{\circ}\text{C}$) with a coefficient of surface heat transfer given by $728 \text{ W/m}^2/^{\circ}\text{C}$. To simulate the removal of water and the subsequent air cooling, the surface boundary condition was chosen to be a heat transfer coefficient given by $7.28 \text{ W/m}^2/^{\circ}\text{C}$ at ambient conditions. A schematic of this configuration is shown in Fig 1.

Table I. Thermal Properties of Shuttle Solid Rocket Motor Materials.

	K (W/m/°C)	Cp (J/Kg/°C)	ρ (Kg/m ³)
Steel	37.4	460.6	7833
NBR	0.268	1591	1290
Fuel	0.381	1214	1763

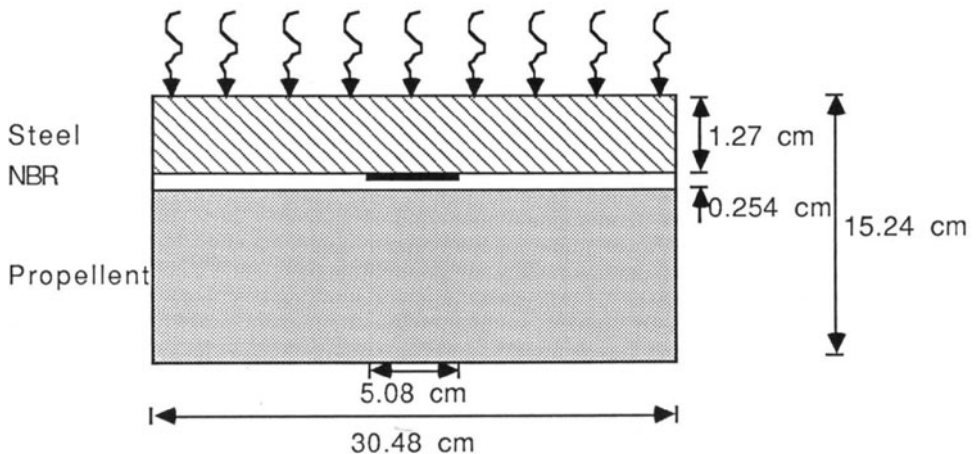


Fig. 1. Typical test geometry. Heating time varies from 15 to 300 seconds.

As the sample is heated, a higher temperature will appear over the disbond than over the rest of the sample. The difference between the highest temperature (which would occur over the disbond) and the temperature at a point in the far field is called the temperature contrast. The temperature contrast across the front face of the sample due to the presence of the buried disbond is unique for each duration of heating. As the heating time is increased, the maximum contrast increases until the sample becomes saturated and the contrast begins to decrease. The family of curves representing the time history plots of the contrast viewed on the front face of the sample for various heating times is shown in Fig. 2. The duration of the application of heat ranges from 15 seconds to 300 seconds, after which the sample is convectively cooled for the remainder of the simulation. Each simulation is separated by 15 second heating intervals. Note that there is a discontinuity in the time derivative of the temperature contrast at the end of the heating phase for samples heated for 45 seconds and longer. The contrast increases rapidly due to the cooling of the regions away from the disbonds at a different rate than the region directly above the flaw. The maximum of each of the curves in Fig. 2 is plotted against heating time in Fig. 3. The maximum of this curve defines the optimum heating time for this particular configuration. Note that the maximum contrast decreases slowly for longer heating times than the optimum. Therefore, a much greater penalty would be paid for underheating than overheating the sample.

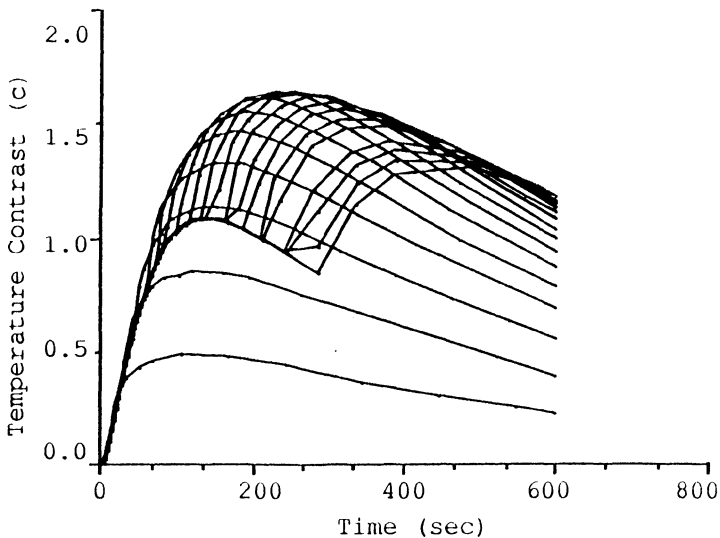


Fig. 2. Temperature contrast vs. time for various durations of heating.

Variations With Disbond Width

A set of simulations were performed to determine the dependence of maximum observed temperature contrast to disbond width. For these simulations the thickness of the steel, NBR insulation and fuel were 1.270 cm, 0.254 cm, and 13.716 cm respectively. A disbond was placed at the NBR and fuel interface (see Fig. 4). The maximum contrast as a function of disbond width from these simulations is shown in Fig. 5.

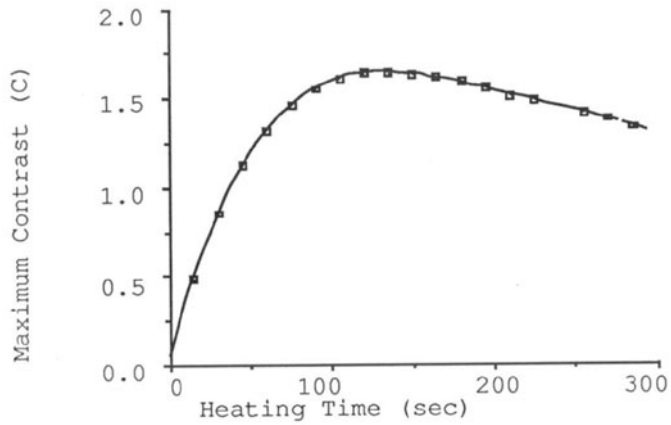


Fig. 3. Maximum temperature contrast for each heating duration.

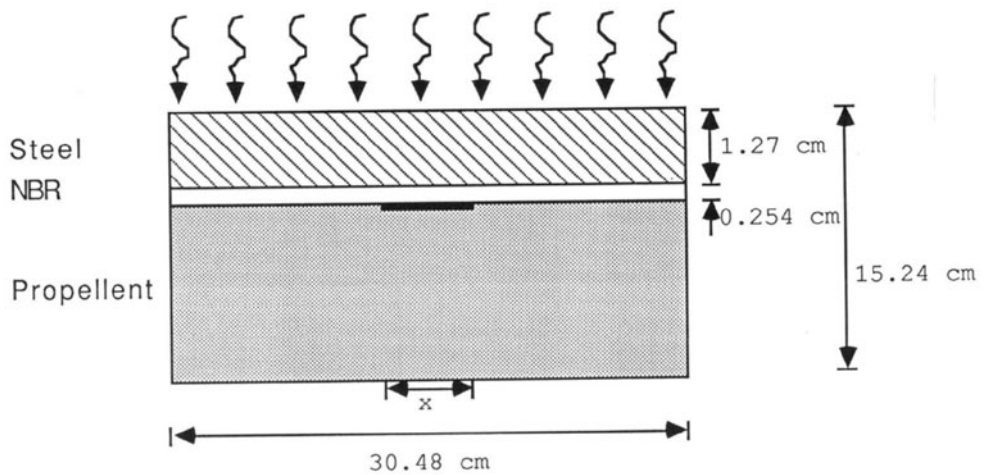


Fig. 4. Typical test geometry for varying disbond width. Sample heated for 60 seconds with a heat transfer coefficient of $728 \text{ W/m}^2/\text{C}$ with subsequent air cooling. Disbond width varies from 0.45 cm to 5 cm.

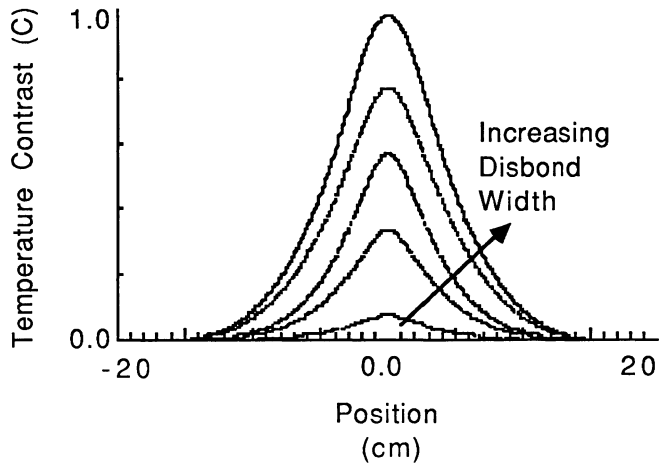


Fig. 5. Temperature contrast profiles across a disbond for various flaw sizes.

The contrasts found from these simulations are within the range found in experiments and are linearly dependent on disbond width (see Fig. 6). The time after removal of the thermal load for maximum contrast tended to increase as the flaw width increased, varying from 100 seconds to 215 seconds after heating for 0.508 cm to 5.080 cm respectively. From these simulations and an analysis of the experiment, it is estimated that a long disbond with a width of .5 cm would be detectable for this configuration. Experimental data is presented in Fig. 7 for comparison. The experimental data does not intersect at zero contrast probably due to uneven heating.

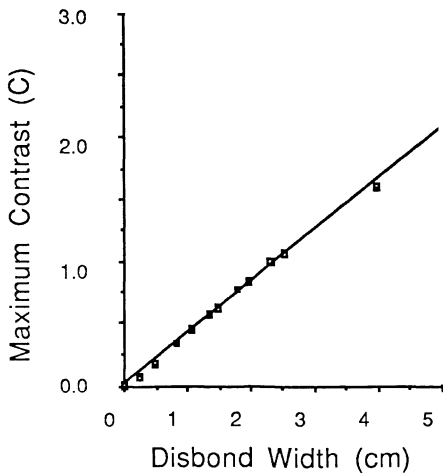


Fig. 6. Maximum contrast as a function of disbond width. Simulation data.

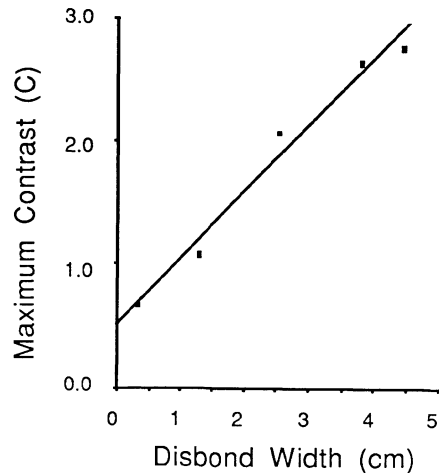


Fig. 7. Maximum contrast as a function of disbond width. Experimental data.

Variations With Steel Thickness

The next set of simulations determined the dependence of the maximum contrast to steel thickness. For these simulations, a two layered material consisting of steel and fuel was used with a 2.54 cm disbond at the interface. The results of this set of simulations is shown in Fig. 8. As expected the temperature profiles spread out as steel thickness increases. For the range of thicknesses investigated, the maximum contrast is inversely proportional to steel thickness as shown in Fig. 9. When the profiles of Fig. 8 are filtered using the method presented by Winfree, et al [3], the flux image remains approximately constant (see Fig. 10) which can then be related to the size of the disbond. From these simulations the maximum thickness of steel through which a 2.54 cm disbond is detectable is 3.5 cm.

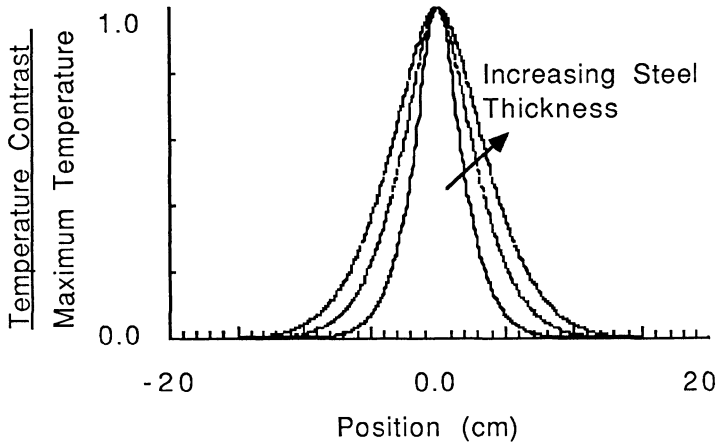


Fig. 8. Normalized temperature profiles for several steel thicknesses.

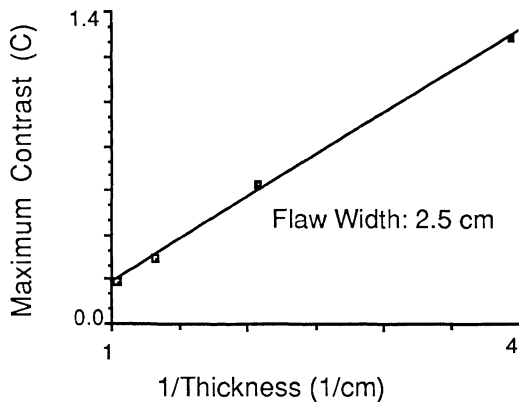


Fig. 9. Maximum contrast as a function of steel thickness.

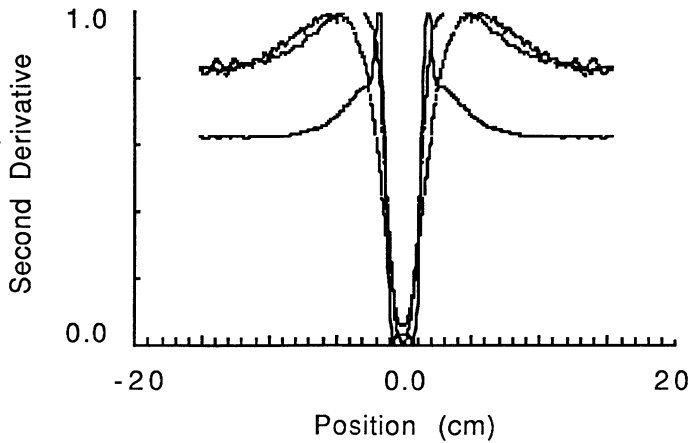


Fig. 10. Filtered profiles (normalized) from Fig. 8. Width of filtered data is related to disbond width.

Variations With Heat Transfer Coefficient

Another parameter of interest is the heat transfer coefficient, h . The geometry for this set of simulations is the same as the geometry that is shown in Fig. 1, where h varied from 72.8 to 7280 $W/m^2/^\circ C$. Variations in heat transfer coefficient showed a maximum contrast at approximately 1000 $W/m^2/^\circ C$ for this configuration (see Fig. 11), after which the contrast slowly decreased then became constant. For the cases where the heat transfer coefficient is large enough to cause penetration of heat quickly into the sample (i.e. for h greater than approximately 728 $W/m^2/^\circ C$, the optimum heating time is shown in Fig. 12.

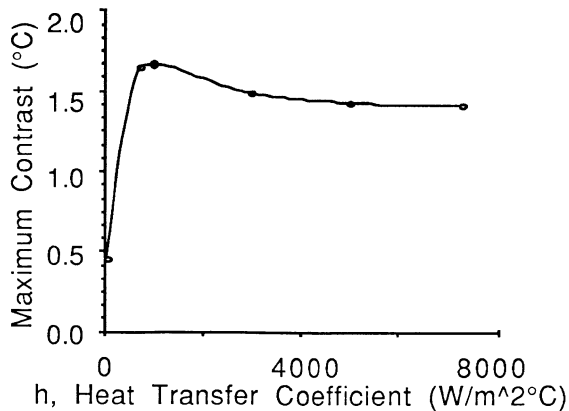


Fig. 11. Maximum contrast as a function of heat transfer coefficient.

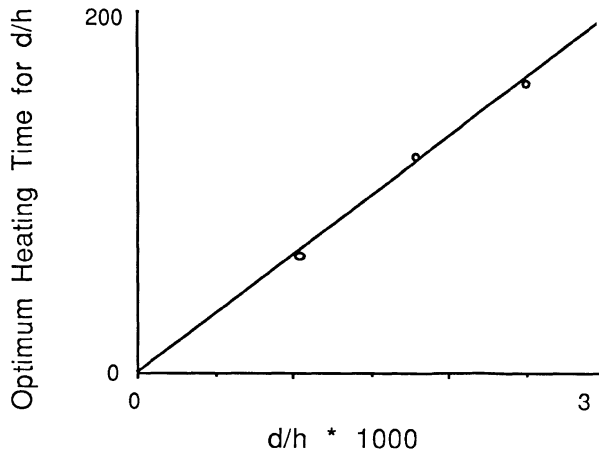


Fig. 12. Optimum heating time as a function of flaw depth and heat transfer coefficient.

From these results, we have found that the optimum heating time is linearly dependent on the ratio of the flaw depth (or the steel thickness) to the heat transfer coefficient as shown in Fig. 12 for this range of surface heat transfer.

CONCLUSIONS

Computational simulations have proven to be an efficient and accurate means of analyzing the effects of boundary conditions on disbond characterization. These simulations have indicated that for convective heating, there is an optimum heating time corresponding to a given steel thickness which is proportional to the ratio of the steel thickness to the heat transfer coefficient. They have also shown that the maximum contrast is linearly proportional to disbond width which could give a relative measure of the sizes of various flaws within a sample. Finally, the maximum contrast is inversely proportional to steel thickness within the range of thicknesses investigated. The maximum thickness of steel through which a 2.54 cm wide disbond is detectable is 3.5 cm.

REFERENCES

1. A. Shapiro, "TOPAZ2D - A Two-Dimensional Finite Element Code for Heat Transfer Analysis, Electrostatics, and Magnetostatics Problems," UCID-20824. Lawrence Livermore National Laboratory, Livermore, California 94550, July, 1986.
2. P. H. James, C. S. Welch, and W. P. Winfree, in Review of Progress in Quantitative NDE, edited by D. O. Thompson and D. E. Chimenti (Plenum Press, New York, 1989), Vol. 8A, pp. 801-809.
3. W. P. Winfree, and P. H. James, from ISA Proceedings, 35th International Instrumentation Symposium, "Thermographic Detection of Disbonds," 1989.